Torque Generated by the Bacterial Flagellar Motor Close to Stall

Richard M. Berry and Howard C. Berg
Rowland Institute for Science, Cambridge, Massachusetts 02142 USA

ABSTRACT In earlier work in which electrorotation was used to apply external torque to tethered cells of the bacterium *Escherichia coli*, it was found that the torque required to force flagellar motors backward was considerably larger than the torque required to stop them. That is, there appeared to be a substantial barrier to backward rotation. Here, we show that in most, possibly all, cases this barrier is an artifact due to angular variation of the torque applied by electrorotation, of the motor torque, or both; the motor torque appears to be independent of speed or to vary linearly with speed up to speeds of tens of Hertz, in either direction. However, motors often break catastrophically when driven backward, so backward rotation is not equivalent to forward rotation. Also, cells can rotate backward while stalled, either in randomly timed jumps of 180° or very slowly and smoothly. When cells rotate slowly and smoothly backward, the motor takes several seconds to recover after electrorotation is stopped, suggesting that some form of reversible damage has occurred. These findings do not affect the interpretation of electrorotation experiments in which motors are driven rapidly forward.

INTRODUCTION

The bacterial flagellar motor is a rotary engine found in the cell envelope of many species of bacteria. It is powered by an inward flux of ions down an electrochemical gradient (reviewed by Macnab, 1996). In most bacteria, each motor drives a helical filament that extends out into the external medium. Rotation of these filaments provides the propulsive force that enables cells to swim. In *Escherichia coli,* several filaments come together to form a bundle that rotates at speeds of a few hundred Hertz and drives the cell body forward at speeds of a few tens of microns per second (Lowe et al., 1987). The cell body counter-rotates at several Hertz. A cell also can be tethered to a surface by a single filament (Silverman and Simon, 1974), in which case its body rotates at speeds up to approximately 20 Hz.

Each motor contains a number of independent torque-generating units believed to comprise the proteins MotA and MotB. The induced expression of wild-type MotA or MotB in tethered but nonrotating *mot* mutants leads to the recovery of torque in a series of equally spaced steps (Block and Berg, 1984; Blair and Berg, 1988). Certain *mot* mutants also lack rings of particles, or studs, that are seen in freeze-fracture electron micrographs of bacterial cell envelopes surrounding depressions of a size similar to the rings thought to be the rotor in the flagellar motor (Coulton and Murray, 1978; Khan et al., 1988). Expression of wild-type Mot proteins restores these particle rings as well as rotation, identifying the particles with torque-generating units.

The relationship between torque and speed is important in assessing models of how the motor functions. By calculating the viscous drag coefficients of the rotating cell body, the torque generated by the motor while running at various speeds in swimming and tethered cells can be estimated. However, the range of motor speeds accessible by these techniques is limited to approximately 50–100 Hz for swimming cells and 0–20 Hz for tethered cells. As well as the intermediate speed range between 20 and 50 Hz, one would like to be able to measure the torque that the motor generates when driven backward or when driven forward up to and beyond its natural maximal speed.

This has been achieved using a technique called electrorotation (Washizu et al., 1993; reviewed briefly in Berg and Turner, 1993), where a controlled torque can be applied to a tethered cell by placing it in a rotating electric field. In experiments performed in our laboratory (Berg and Turner, 1993; Berry et al., 1995), the rotating electric field was generated between four tungsten electrodes, arranged in a cross around a gap at the center of approximately 70 μm, and held at a distance of approximately 10 μm from the surface on which cells were tethered. Opposing pairs of electrodes were driven at 2.25 MHz with sinusoidal voltages 90° out of phase, and it was possible to make cells rotate at speeds approaching 1000 Hz. The experimental protocol of Berg and Turner is illustrated in Fig. 1 *a*. For various electrorotation power levels, P (proportional to voltage squared, which is proportional to torque), the rotation rate of the cell was measured, first with the motor intact (filled symbols) and later with the motor broken (such that the cell no longer rotated on its own, open symbols). The difference in rotation rates with the motor intact or broken, called the speed offset, is proportional to the torque generated by the motor when intact. Two main conclusions were reached, based upon results obtained from nearly 100 cells. First, motors generated approximately constant torque rotating forward at speeds up to several hundred Hertz, depending on temperature. At higher speeds, torque was reduced, until at the highest speeds the motor resisted forward rotation. Second, the torque required to drive cells backward was significantly larger than the torque required to stop them

Received for publication 11 July 1996 and in final form 17 September 1996.

Address reprint requests to Dr. Horard C. Berg, Molecular and Cellular Biology, Harvard University, 16 Divinity Avenue, Cambridge MA, 02138. Phone: 617-495-0924; Fax: 617-496-1114; E-mail: hberg@biosun.harvard.edu.

0006-3495/96/12/3501/10 $2.00

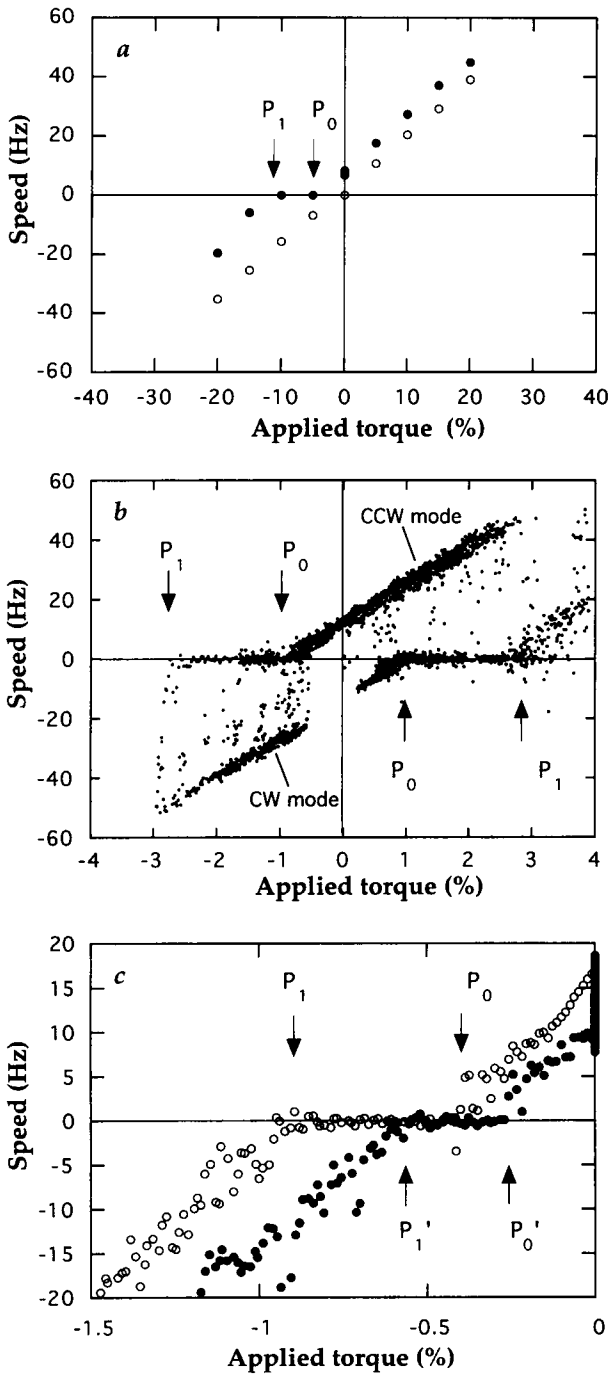

FIGURE 1 (*a*) Rotation rate of a tethered cell as a function of electrorotation strength, taken from Berg and Turner (1993). Applied torque (or electrorotation strength, P) is proportional to the square of electrode voltage and is given as a percentage of the maximum possible for one of several power supply configurations. A positive sign denotes an applied field that tends to drive the cell forward, a negative sign one (rotating in the opposite direction) that tends to drive the cell backward. Cell speed (rotation rate) is obtained as the peak in the power spectrum of data from a linear-graded filter apparatus. This cell was stopped by an electrorotation strength of -5% (P_0), but more than -10% (P_1) was needed to make it rotate backward. (*b*) Rotation rate versus electrorotation strength for a cell with a motor able to generate torque in either direction, taken from Berry et al. (1995). In the CCW mode, forward rotation is counterclockwise (positive); in the CW mode, it is clockwise (negative). In either mode, more power is required to drive the cell backward than to stop it. (*c*) Rotation rate versus electrorotation strength before and after partial breaking, taken from Berry et al. (1995). Initially, the cell rotated at 17 Hz without electrorotation; it gave the curve marked by open symbols with electrorotation. After progressive breaking, the curve marked by closed symbols was obtained. This motor showed the same behavior as those in *a* and *b*, both before and after breaking, with the ratio P_1/P_0 remaining approximately constant.

from spinning forward. In other words, there was a barrier to backward rotation. This can be seen in Fig. 1 *a*, where an electrode power level of -5% (P_0) was enough to stop the cell, but more than -10% (P_1) was needed to make it spin backward. It was also noted that cells driven backward often broke, either catastrophically (sudden irreversible reduction to zero torque) or progressively (progressive reduction to zero torque followed by progressive recovery in a few minutes).

A more detailed study of cells driven backward (Berry et al., 1995) demonstrated that the relationship between applied torque and speed was symmetrical in cells the motors of which switch their natural direction of rotation (Fig. 1 *b*). It was also shown that progressive breaking involves the removal of individual torque-generating units, of which the motor is thought to contain 8 (Blair and Berg, 1988) or perhaps up to 16 (Block and Berg, 1984; Berry et al., 1995). The torque generated by partially broken motors with a smaller number of working units was reduced by a constant factor at all speeds (Fig. 1 *c*).

The evidence that the barrier was an intrinsic feature of the torque-generating mechanism of the motor seemed compelling. The symmetry shown in Fig. 1 *b* argued against an explanation in terms of cells sticking to the surface when driven in one direction. The behavior of partly broken cells (Fig. 1 *c*) indicated that the barrier, or more specifically the ratio P_1/P_0, was attributable to individual torque-generating units. Cells stalled by electrorotation for long periods of time would creep backward as slowly as one revolution per several minutes, as if they were being pushed over high energy barriers to backward rotation. When the torque was varied between P_0 and P_1, as defined in Fig. 1 *a*, cells moved back and forth as expected if the motor were locked and the tether were being wound and unwound. The estimated tether compliance fell in the middle of the range measured previously using optical tweezers (Block et al., 1989). Furthermore, it seemed reasonable that cells should break when pushed backward if the torque sustained by the motor in this regime were considerably greater than in cells running forward. And a barrier to backward rotation had been predicted by a theoretical model of the motor mechanism (Meister et al., 1989).

A closer investigation of cells stalled by electrorotation for long periods of time, however, revealed a number of inconsistencies. Many cells stalled at particular angles, often at two angles roughly 180° apart. When electrorotation was stopped after stalling cells with P between P_0 and P_1, cells often rotated slowly or not at all for a second or two before getting up to speed. If stalled cells really were resisting electrorotation with a torque considerably greater

than that generated when running forward with no electrorotation, this would wind the tether up more tightly than in the running cell. Torque in the tether is always the same as the torque supported by the motor, and in the absence of electrorotation, it is directly proportional to cell speed. Thus, cells should have rotated transiently faster when the electrorotation was stopped, not slower. These and other inconsistencies in the data led us to test whether there might be an alternative explanation for the results of the electrorotation experiments.

An alternative interpretation of the electrorotation experiment

In an electrorotation experiment, the following balance of torque applies:

$$T_m + T_e - f\omega = 0,$$

where T_m, T_e, f, and ω are the torque generated by the motor, the torque generated by electrorotation, the rotational frictional drag coefficient, and the angular velocity of the cell body, respectively. At stall, $\omega = 0$, and $T_m = -T_e$. If T_m and T_e are independent of the orientation of the cell, as assumed in our earlier work, and the cell remains stalled as T_e is increased, then T_m must also increase, indicating a barrier to backward rotation. But what are the consequences if T_e, T_m, or both, vary with cell orientation, θ? To find out, we write $T_m = T_m(\theta)$ and $T_e = Pg(\theta)$, where P is the oscillator power setting and $g(\theta)$ is a factor specifying the angular dependence of applied torque. In this case, the power setting required to stall the cell varies with angle: $P_{stall} = -T_m(\theta)/g(\theta)$.

Fig. 2 *a* shows P_{stall} for a hypothetical case in which T_m = constant = 10 and $g(\theta) = 1 + 0.3\cos(2\theta)$, i.e., $P_{stall} = -10/[1 + 0.3\cos(2\theta)]$. The horizontal lines indicate different settings of the electrorotation control P_0, P_a, and P_1. At P_0, the torque due to electrorotation is just sufficiently negative to stall the cell at 0° or 180°. If the power level is made steadily more negative, as in earlier experiments (Berry et al., 1995), the cell will remain stalled, moving slowly backward with P (for instance, to either 300° or 120° at $P = P_a$, as shown by the filled squares in Fig. 2 *a*). At $P = P_1$, the cell will move to 270° or 90°. At power levels more negative than P_1, the cell will rotate backward, because now the amplitude of the applied torque is larger than the motor torque at all angles. The domains shown by the dashed lines are not stable. If a cell finds itself in one of these domains, it will rotate until coming to equilibrium in one of the adjacent domains, shown by the solid lines. Fig. 2 *b* shows the average speed of the cell versus P (heavy line) for the same hypothetical case, calculated via a computer simulation of the equation of motion for the cell. The curves in Fig. 2 *b* are similar to those in Fig. 1. Fig. 2 *c* shows results of the same simulations as Fig. 2 *b*, over a larger range of electrorotation strengths. Curves for broken and intact cells are parallel at high speeds in either direction.

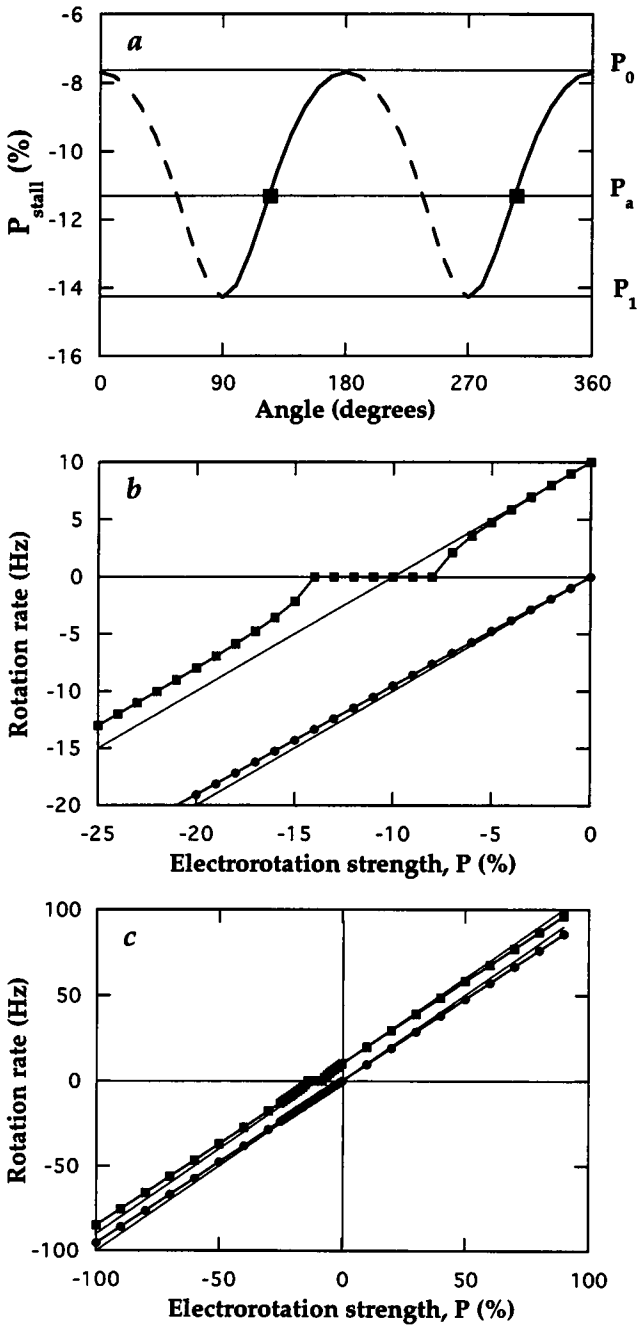

FIGURE 2 (*a*) Dynamics of a cell for which the electrorotation strength required for stall, P_{stall}, varies with the angle of the cell body. In this example, we assume that the motor generates constant torque (equal to the mean electrorotation torque at $P = 10$) and that the torque applied by electrorotation equals $P[1 + 0.3\cos(2\theta)]$. For values of P between P_0 and P_1, the cell will be stalled at points such as those marked by squares on portions of the P_{stall} curve with positive slope (——). (*b*) Rotation rate versus P for the cell shown in *a*, obtained by computer simulation. The curve passing through the origin is for the same cell with no motor torque, as after a catastrophic break. The light lines are for the same cell, either intact or broken, with no angular variation in electrorotation torque. (*c*) As for *b* but over a wider range of electrorotation strengths.

This indicates that angular variation in P_{stall} does not affect the conclusion of earlier electrorotation experiments, that motor torque is independent of speed up to more than 100

Hz at room temperature (Washizu et al., 1993; Berg and Turner, 1993).

A similar predicament arises if the angular dependence resides with the motor and not the electrode array. Suppose, for example, that $T_m(\theta) = Qh(\theta)$, and $T_e = P$, with Q = constant = 10 and $h(\theta) = 1/[1 + 0.3\cos(2\theta)]$. Then $P_{stall}(\theta) = -10/[1 + 0.3\cos(2\theta)]$, as before. So one observes the same angular variation in the power required to stall the cell, even though there is no barrier to backward rotation.

In the sections that follow we demonstrate that such angular variations exist and that they accurately predict the apparent barriers observed if we assume that the motor torque-speed relationship is constant, or linear, through zero speed. One possible source of these angular variations is an imbalance in the electrode array. However, angular variations in motor torque or small barriers to backward rotation cannot be ruled out. Experiments using other methods will be required to settle this issue.

MATERIALS AND METHODS

Electrorotation of cells

Experimental methods were as described previously (Berg and Turner, 1993; Berry et al., 1995) with the following exceptions. All cells were of the counterclockwise-rotating strain KAF95 (Berg and Turner, 1993). Electrodes were platinum-iridium wires of 51 μm outer diameter insulated with a 12.5-μm Teflon coating (7760; A-M Systems, Everett, WA). They were mounted upon a platform attached to the microscope stage, and cells were tethered to a moveable glass coverslip resting upon this platform, suspended approximately 10 μm away from the electrodes. This arrangement allowed a choice of microscope objectives, and we used phase-contrast objectives with either 20× or 40× magnification. All experiments were performed at room temperature.

The oscillator used earlier was replaced by one with less distortion, built around a voltage-programmable oscillator chip (Maxin MAX038, Sunnyvale, CA). Its output (the sine signal) was fed through a multiplier (Analog Devices AD734, Norwood, MA) and integrator to generate the cosine signal, with the voltage used to program the oscillator serving as the multiplicand. This arrangement gave sine and cosine signals of equal amplitude, independent of frequency. The delay introduced by the multiplier was offset, on the sine side, by a delay line. In some experiments (those in Figs. 3, 4, 7, and 8), the wide-band push-pull amplifiers that normally followed the oscillator were removed, so that the required power settings (P values) were approximately an order of magnitude larger than before.

The angular dependence of P_{stall} was estimated as follows. The linear-graded filter (LGF) apparatus (Berg and Turner, 1993) was used to record the angle of the cell body over a large number of revolutions while the cell spun on its own or was slowed down by electrorotation. For each value of P, the speed of the cell was obtained as the slope of cell angle versus time, and data points were sorted by angle into 20 bins, each 18° wide. For each value of P and angle, the average speed was computed, and the standard error in the speed was taken as an estimate of the uncertainty. Then, for each angle, a least-squares linear fit of average speed versus P was found, and the zero-speed intercept and the error of the intercept were taken as estimates of P_{stall} and the uncertainty in P_{stall}, respectively.

For the analysis of data from cells stalled for extended periods of time, the X- and Y-LGF signals were converted to the cosine and sine of the cell angle by superimposing a circle upon a plot of Y versus X and adjusting the center and radius of the circle by eye to match the data. This also allowed the selection of data for which the cell was well aligned in the LGF, so that the (X, Y) signal was circular.

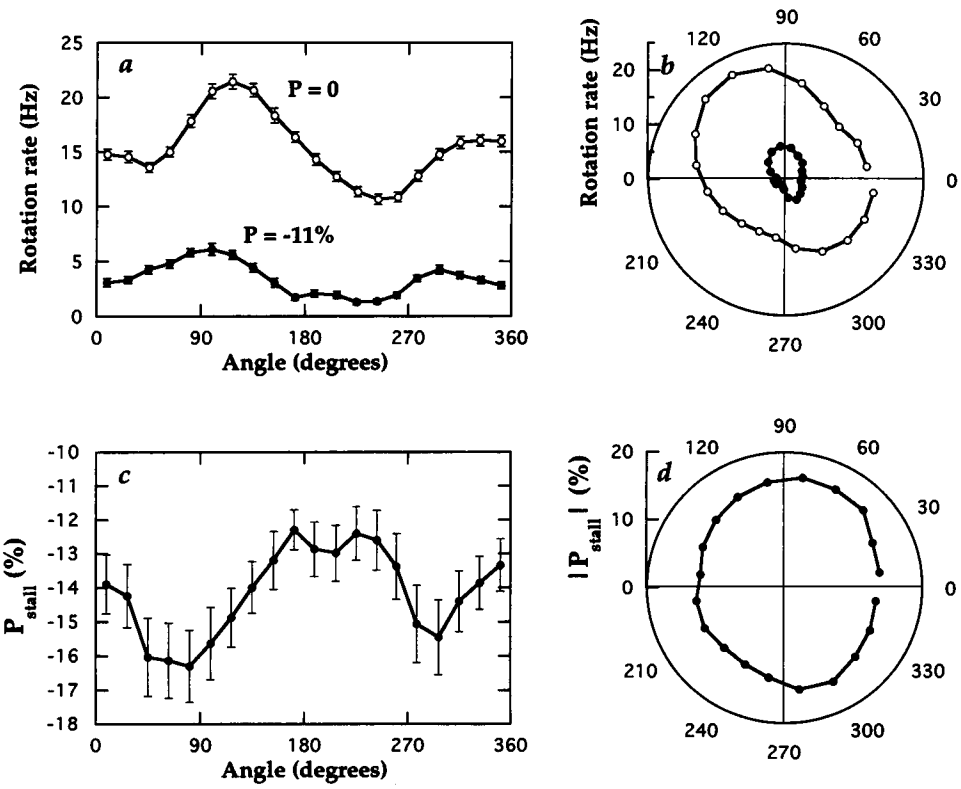

FIGURE 3 (*a* and *b*) Mean rotation rate versus angle for a tethered cell at $P = 0$ and $P = -11\%$. The rate of rotation of the cell without electrorotation and the amount by which electrorotation slows the cell both vary considerably with cell angle. (*c* and *d*) Values of P_{stall} estimated from the data in *a* and *b*. For each angle, P_{stall} was taken as the zero-rotation-rate intercept of a least-squares linear fit of rotation rate versus P (in this particular case, where there were only two points per angle, simply the line drawn through the two points).

Computer simulations

The equation of motion for a cell was integrated numerically in LabView (National Instruments, Austin, TX) using the Euler method. For Fig. 2 *b*, we assumed constant motor torque and frictional drag coefficient, and an electrorotation torque that varied with angle as described above. For Fig. 4 *a*, we assumed that cell speed is a linear function of P at each angle, specifically, that $\omega(P,\theta) = \omega_0(\theta)[1 - P/P_{stall}(\theta)]$. $\omega_0(\theta)$, the speed of the cell with $P = 0$, was obtained from Fig. 3 *a*, and P_{stall} was obtained from Fig. 3 *c*. Then the rotation of the cell was simulated by numerical integration of the equation $d\theta/dt = \omega(P, \theta)$. Linearity between cell speed and P follows if the motor torque is either independent of speed or if it varies linearly with speed, in either case without a barrier to backward rotation.

RESULTS

To test the alternative explanation for the apparent barriers to backward rotation in flagellar motors, we obtained estimates of P_{stall} as a function of angle for a number of tethered cells and then, as in the previous experiments, applied increasing torque against the motor using electrorotation. This allowed us to compare the apparent barrier measured for a particular cell to the apparent barrier predicted for the same cell by the alternative explanation. We used the same strain (KAF95) and tethering technique as in the earlier work (Berg and Turner, 1993).

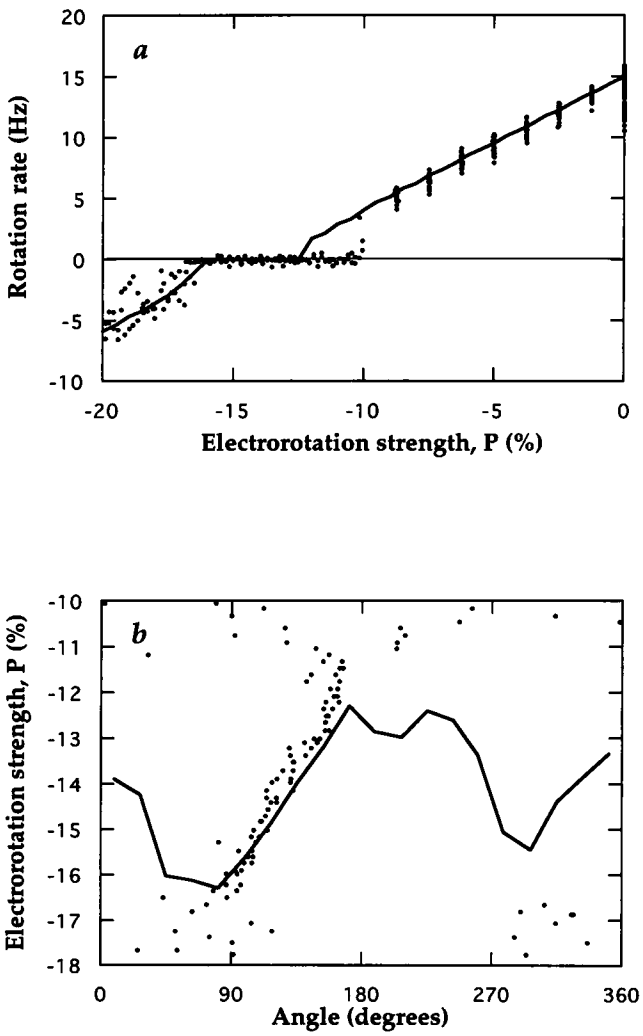

FIGURE 4 (*a*) Rotation rate versus electrorotation strength for the cell shown in Fig. 3. The dots show measured rotation rates, and the line shows rotation rates predicted by a computer simulation based on the data of Fig. 3, *c* and *d*, and the dynamics described in Fig. 2. (*b*) The same data plotted as P versus cell angle and superimposed upon the P_{stall} versus angle curve from Fig. 3 *c*. The cell stalled at points on the portion of the P_{stall} curve with positive slope, as predicted in Fig. 2 *a*.

Fig. 3 *a* shows the speed of one cell with electrorotation strengths (P) equal to 0 and -11%. Notice that the speed of the cell varied considerably within a single revolution, even in the absence of electrorotation. Possible causes of this include angular variations in the motor torque and angular variations in the frictional drag coefficient, either due to asymmetry in the tethering geometry or direct interactions between the cell body and the tethering surface. With external torque applied against the motor, the cell rotated more slowly at all angles, and the amount by which it is slowed varied with angle. We obtained an estimate of P_{stall}, shown for this cell in Fig. 3 *c*, as the zero-speed intercept in a line fit of speed versus P, as described in Materials and Methods. Fig. 3, *b* and *d*, are polar plots of the data in Fig. 3, *a* and *c*, respectively.

From Fig. 3 *c*, we would predict that the cell would be stalled by electrorotation between $P_0 = -12\%$ and $P_1 = -16.5\%$. Fig. 4 *a* shows the speed of this cell as a function of P. The electrorotation strength was first increased incrementally from $P = 0$ to $P = -9\%$, in the fashion of Berg and Turner (1993), and later was increased smoothly, from -10 to -20%, in the fashion of Berry et al. (1995). The solid line shows predicted mean speeds for this cell, calculated by a computer simulation based on the data of Fig. 3 and assuming that the motor torque is a linear function of speed (i.e., has no barrier) over the range of speeds covered; see Materials and Methods. Fig. 4 *b* shows P as a function of the angle of the cell, superimposed upon the calculated values of P_{stall} from Fig. 3 *c*. This shows that the cell did indeed dwell on the portions of the P_{stall} curve with positive slope, as predicted in Fig. 2 *b*. The cell stopped rotating forward at less negative values of P than predicted, which might be explained if the motor underwent partial breaking during these runs, thus reducing the actual magnitude of P_{stall}. That partial breaking actually did occur is demonstrated by the points in the vicinity of 12 Hz on the $P = 0$ axis of Fig. 4 *a*, where the cell rotated at a reduced rate after being pushed backward by electrorotation.

Fig. 3 shows that the strength of electrorotation, P, required to stall one particular cell does vary considerably with cell angle, and Fig. 4 shows close agreement between the measured speeds and angles of that cell and those predicted if there is no barrier to backward rotation. To confirm this agreement, we compared measured and predicted behavior in an additional 13 cells. Fig. 5 *a* shows measured versus predicted values of the magnitude of the electrorotation strength required just to stall a cell ($|P_0|$, filled symbols) and to make it rotate backward ($|P_1|$, open symbols). Measured values were read off graphs of speed

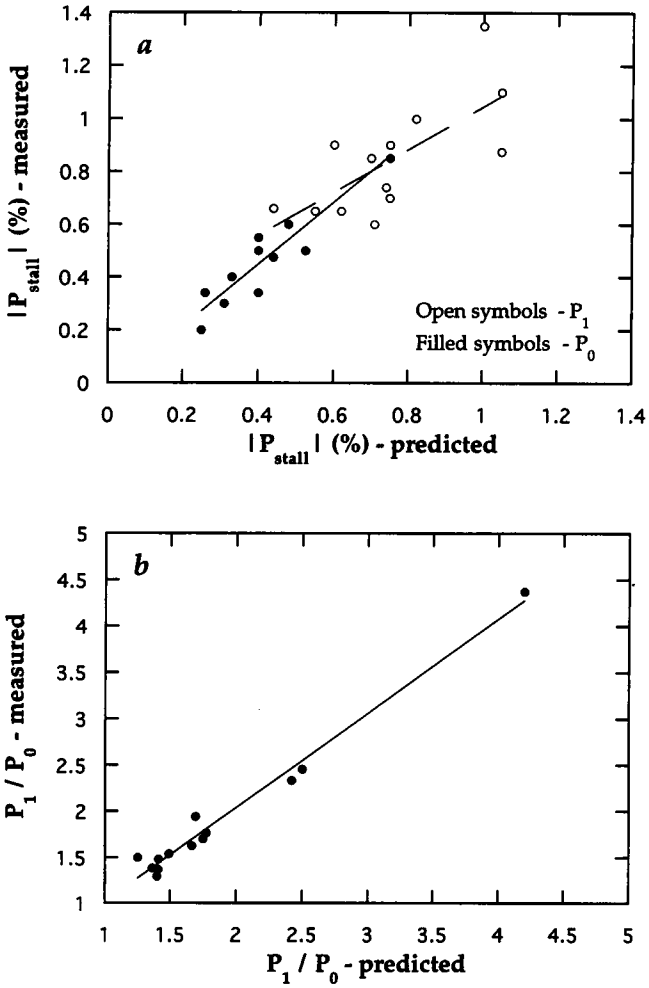

FIGURE 5 (*a*) Measured versus predicted values of P_0 (●) and P_1 (○) for 13 different cells. The solid line is a least-squares fit to the values of P_0, and the dashed line is a similar fit for P_1. The values of P here and in Fig. 6 are smaller than in the other figures, because the oscillator outputs passed through wide-band push-pull amplifiers. (*b*) Measured versus predicted values of the ratio P_1/P_0 for the data shown in *a*. The line is a least-squares fit.

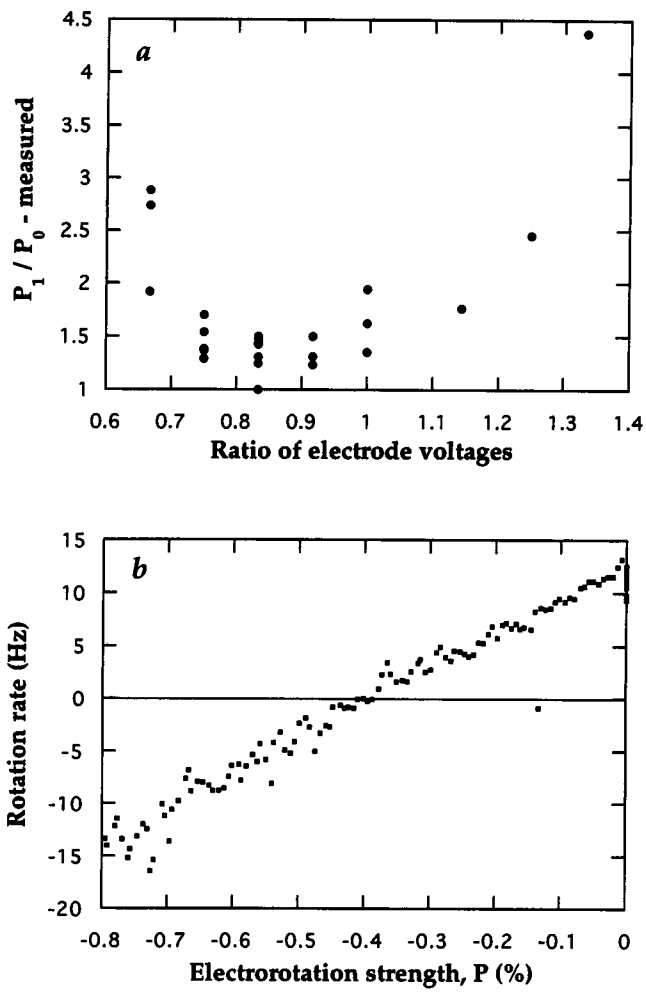

FIGURE 6 (*a*) The measured ratio P_1/P_0 plotted against the ratio of amplitudes of the voltages applied to the two orthogonal pairs of electrorotation electrodes. Ratios were measured for the 13 cells of Fig. 5 and an additional 8 cells. The electric fields in the x and y directions experienced by a cell are proportional to the voltage between each pair of electrodes divided by the distance between the pair. Unequal voltage amplitudes produce an elliptical rather than a circular rotating field at the cell, which presumably leads to angular variation in the electrorotation torque. The P_1/P_0 ratio varied systematically with the ellipticity of the rotating electric field. (*b*) Rotation rate versus P for the cell, shown in *a*, with a P_1/P_0 ratio of 1. The motor in this cell showed an approximately linear dependence of speed upon applied torque, with no barrier to backward rotation.

versus P similar to Fig. 1 *a* or Fig. 4 *a*. Predicted values were taken as the minima and maxima in graphs of P_{stall} versus angle, similar to Fig. 3 *c*. Straight lines are least-squares fits to the $|P_0|$ and $|P_1|$ data. We see that there is good agreement between measured and predicted values over a wide range. Fig. 5 *b* shows for the same data set measured versus predicted sizes of the apparent barrier, defined as the ratio P_1/P_0. Again, we see close agreement between measurement and prediction, with the least-squares line fit almost identical to a line of unit slope.

To show that angular variations in the torque due to electrorotation can be significant, we measured apparent barriers to backward rotation for a number of additional cells while adjusting the relative amplitude of the voltage signals applied to the two pairs of electrodes. Fig. 6 *a* shows the measured ratios P_1/P_0 plotted as a function of the ratio of signal amplitudes. The apparent barriers varied systematically with the ellipticity of the rotating electrical field, but, with the exception of one cell (shown in greater detail in Fig. 6 *b*), they were never zero. When the ellipticity of the rotating field was large, most cells showed two evenly spaced maxima in P_{stall}, at roughly fixed angles relative to the electrode array. When the ellipticity was small, on the other hand, two maxima were not evident.

The fact that the minimum in P_1/P_0 occurred with a ratio of electrode voltages between 0.8 and 0.9 suggests an asymmetry in electrode spacing. The fact that its average value in this region was approximately 1.3 tells us that the apparent barrier cannot be accounted for entirely by imbalance between the X and Y components of the electric field. Either

the electric field is asymmetric for other reasons, motor torque depends on angle, or there is a barrier to backward rotation, albeit one substantially smaller than estimated earlier (Berg and Turner, 1993, where the P_1/P_0 ratio was approximately 2.2, on average).

Behavior of cells under prolonged electrorotation torque

The analysis presented above indicates that most of the observations previously taken as evidence for barriers to rotation can be explained, instead, as a result of the angular variation in the electrorotation strength required to stall a cell. However, the analysis does not explain the behavior of many cells that are stalled by electrorotation for extended periods of time. If, when stalled, the motor generates torque that is independent of angle, or torque that depends on angle but is time invariant, then we would predict that the cell would remain indefinitely at one of the stable points marked by the squares in Fig. 2 *a*. Berg and Turner (1993) reported that under such conditions cells actually rotate very slowly backward, sometimes taking several minutes to complete a single revolution. To investigate this phenomenon more closely, we recorded cell angles using the LGF apparatus while applying a wide range of electrorotation torque to stall cells for 64 s at a time. Some cells actually stuck at fixed angles, as predicted by Fig. 2 *a*, but others rotated slowly backward.

We distinguished two different types of backward rotation: sudden 180° jumps at randomly spaced time intervals and slow, smooth rotation. Fig. 7 *a* shows a cell rotating in 180° jumps during a run in which constant electrorotation was applied at $P = -12\%$, beginning at $t = 4$ s and ending at $t = 68$ s. The same data are shown in the right panel of Fig. 7 *b*, with cell angles mapped into a single period from 0° to 360°. The left panel of Fig. 7 *b* shows the calculated values of P_{stall} as a function of cell angle, obtained before the cell was pushed hard enough to stall it at any angle. The vertical line and squares in the left panel mark $P = -12\%$ and the corresponding stable points, respectively. The cell jumped abruptly between fixed angles close to the predicted stable points.

Fig. 8 *a* shows an example of slow, smooth rotation. The left panel shows the calculated values of P_{stall} as a function of cell angle, as in Fig. 7 *b*, and the central panel shows the angle of the cell against time during two runs in which constant electrorotation was applied, first at $P = -15\%$ and then at $P = -16\%$. Vertical lines and squares in the left panel mark these values of P and the corresponding stable points. Although the cell did move more slowly near the stable points, it did not actually stop. Instead, it actually moved smoothly through substantial fractions of a revolu

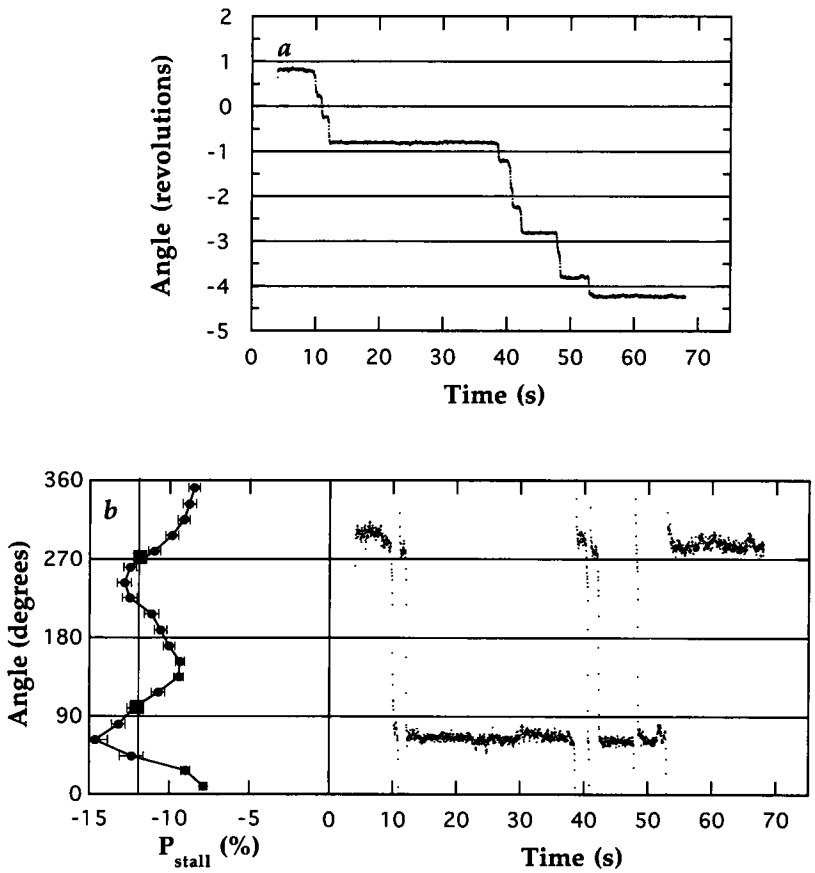

FIGURE 7 (*a*) Cell angle versus time for a tethered cell subjected to electrorotation for 64 s continuously. Electrorotation was applied at $t = 4$ s and removed at $t = 68$ s, with $P = -12\%$. The cell made 10 jumps of approximately one-half of a revolution each. (*b*) On the left side are the predicted values of P_{stall} versus angle for the same cell. The vertical line marks $P = -12\%$, and the squares show the predicted stable points. The right side is as in *a* but showing more clearly the two angles at which the cell stopped.

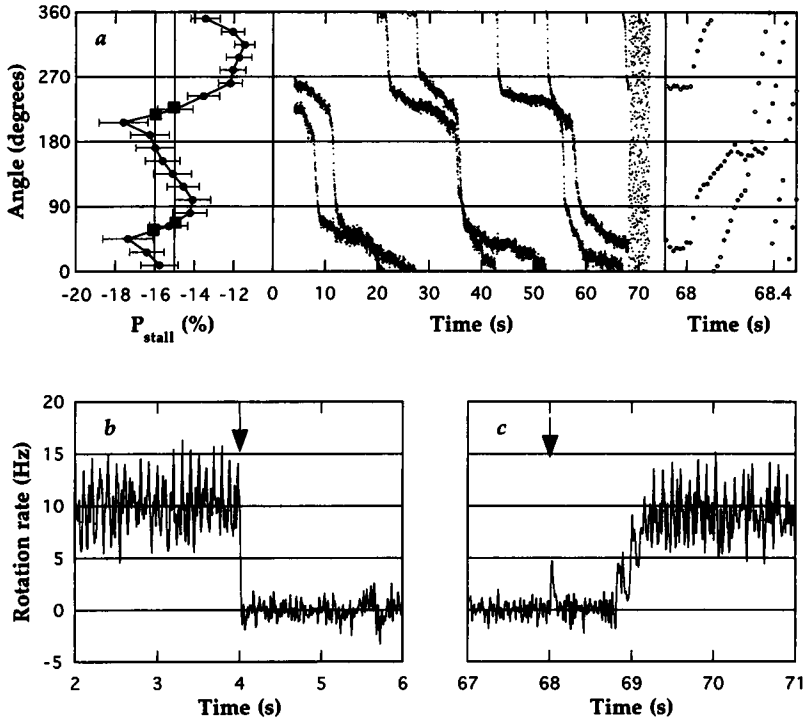

FIGURE 8 (*a*) In the center is cell angle versus time for a tethered cell subjected to electrorotation for 64 s continuously in each of two separate runs. Electrorotation was applied at $t = 4$ s and removed at $t = 68$ s with $P = -15\%$ in the first run and $P = -16\%$ in the second run. The cell made approximately three full revolutions in each run. On the left are the predicted values of P_{stall} versus angle for the same cell. The vertical lines mark $P = 15\%$ and $P = 16\%$, and the squares show the predicted stable points for each case. On the right is angle versus time on an expanded time scale, showing the behavior of the cell just after electrorotation was stopped. (*b* and *c*) Rotation rate versus time for the same cell as in *a* in a similar run with $P = -13\%$. (*b*) Rotation rate around $t = 4$ s. (*c*) Rotation rate around $t = 68$ s. The arrows mark the times at which electrorotation was started ($t = 4$ s) and stopped ($t = 68$ s).

tion, as, for example, between 10 and 25 s. The right panel shows cell angle versus time for the same runs but on an expanded time scale. In both runs when the electrorotation was stopped, the cell rebounded through about one-third of a revolution in approximately 0.1 s before stopping for a short while and then starting to rotate forward. The time course of the rebound was similar to that observed by Block et al. (1989), who wound up the tethers of locked cells using an optical trap and watched them unwind after the trap was turned off. Fig. 8, *b* and *c* shows speed versus time for the same cell before and after a run at $P = -13\%$. In between, the cell completed one revolution (data not shown). When the field was turned on (arrow, Fig. 8 *b*), the cell decelerated at once. When it was turned off (arrow, Fig. 8 *c*), there was a brief rebound (the spike of positive speed at $t = 68$ s), followed by almost a second before the cell started to rotate forward. Over the course of the next second, the cell accelerated to a steady speed significantly smaller than its initial speed.

When cells rotated in 180° jumps, they tended to start up instantly at full speed. When cells rotated smoothly and slowly backward, on the other hand, they invariably started up slowly after release, although not always at zero speed. Both types of behavior are compared in the histograms of Fig. 9.

DISCUSSION

Our main conclusion is that the apparent barrier to backward rotation in the bacterial flagellar motor, inferred from earlier experiments, is probably an artifact due to an angular dependence in the power level required to stall a cell. The angular variation in P_{stall} accurately predicted the apparent barriers observed, over a wide range of barrier sizes, under the assumption that the motor torque-speed relationship is constant, or linear, through zero speed. Angular variation in P_{stall} could be due to angular variation in the torque generated either by electrorotation or by the motor itself. When the rotating electric field was deliberately made elliptical rather than circular, two evenly spaced maxima were observed in P_{stall}, as expected. When the ellipticity of the rotating field was minimized, evenly spaced maxima were no longer evident. The small and irregular variation in P_{stall} that remained might be due to irregularities in the shape or position of the electrodes, in the dielectric environment of the cell, or in the rotational symmetries of the rotor and stator.

Our conclusion that the motor torque is independent of speed or varies linearly with speed, at low speeds, is similar to that of Washizu et al. (1993), who also measured the rotation rate of tethered cells under electrorotation and found that the motor generated constant torque. Their tethering technique, means of field generation, and electrode geometry were different, and they used *Salmonella typhimurium* instead of *E. coli*. However, they also saw a number of cells that exhibited an apparent barrier to backward rotation (S-I. Aizawa, personal communication), which they ignored on the assumption that these cells were sticking to the tethering surface. They also reported that for many cells "especially when (rotation rate) was small, the rotation appeared to slow down at a particular angle once a revolution," consistent with a variable P_{stall}. Their published data on the torque-speed relationship were based on a single cell, and although no apparent barrier is demonstrated, the data

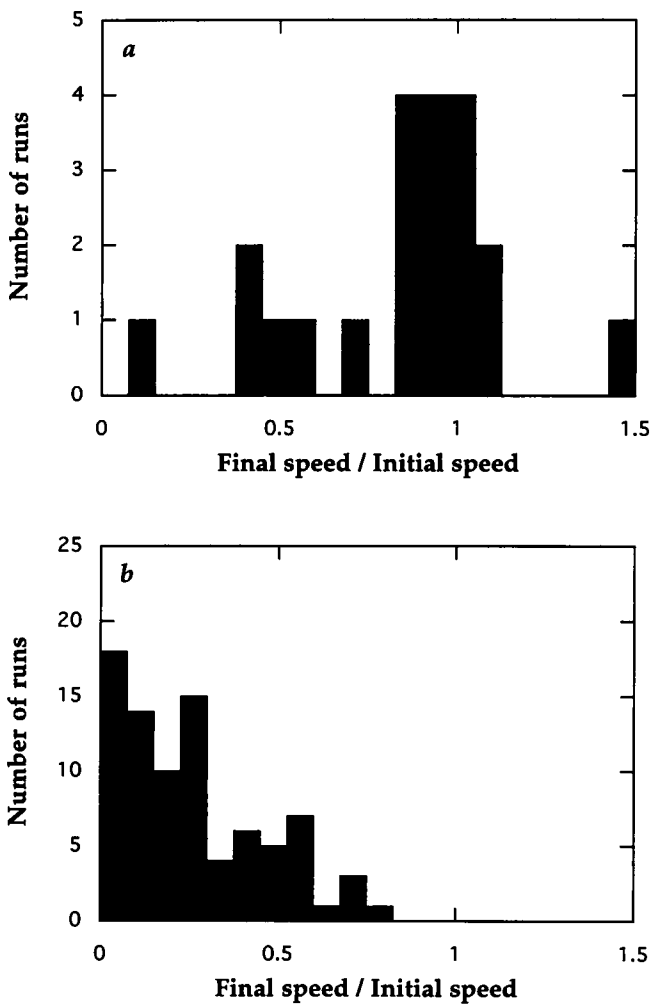

FIGURE 9 (*a*) Distribution of speed ratios for 21 runs in which cells moved backward in jumps of 180°. The final speed was measured between 0.1 and 0.2 s after the electric field was turned off, and the initial speed was measured between 4 and 0 s before the electric field was turned on. (*b*) As in *a* but for 84 runs in which cells rotated smoothly and slowly backward. Our definition of smooth, slow rotation was steady rotation through more than one-tenth of a revolution over the course of 5 s or longer. The data in *a* and *b* were obtained from 22 different cells; 3 cells moved in jumps in all runs (*a*), 14 rotated smoothly backward in all runs (*b*), and 5 rotated smoothly in some runs and made jumps in others (*a* and *b*).

are too sparse to rule out the presence of such a barrier. Only one point is shown where the cell is stalled and none where it rotates backward at less than 20 Hz.

We found that most cells rotated slowly backward when stalled for extended periods by electrorotation, some in jumps of 180° (Figs. 7 and 9 *a*) and others slowly and smoothly (Figs. 8 and 9 *b*). Although the majority of our data show cells rotating smoothly, this may reflect selection bias rather than a genuine predominance of smooth rotation. At the time these experiments were performed, our goal was to study smooth rotation, and we tended to stop collecting data on cells that either did not rotate or that rotated in jumps of 180°. We suspect that backward rotation in jumps of 180° is due to temporal fluctuations in motor torque. If, for example, the number of active torque-generating units in the motor varies, then from time to time the motor torque will be reduced far enough to allow the cell to rotate backward past a maximum in $|P_{stall}|$. If the torque returns to higher levels within a fraction of a second, the cell will stop at the next stable point (Figs. 2 *a* and 3 *c*), progressing in randomly timed jumps of approximately one-half of a revolution each as shown in Fig. 7. This behavior was reproduced in computer simulations, in which each torque-generating unit was assumed to go on and off at random, with fixed rate constants. With rate constants on the order of 1 to 10 per second, the average speed varied approximately exponentially with torque, as was observed in the majority of cells. Smooth backward rotation might be explained if these cells were being pushed backward over fixed energy barriers to rotation. The rate of crossing such an energy barrier is proportional to $\exp[A\phi/kT]$, where ϕ is the angle through which an applied torque, A, does work in surmounting a barrier. If the motor were working normally, this would have told us about the interaction potential between the rotor and the stator, and therefore something about the torque-generating mechanism. However, the delayed recovery of normal torque when electrorotation was stopped (Figs. 8 *c* and 9 *b*) indicates that when cells rotated smoothly backward their motors were in an abnormal, damaged state. This damage might be caused by off-axis torques or lateral forces that disrupt the relative positions of the rotor and stator and therefore the interactions that generate motor torque. Thus, although we may learn something about the structure of the motor from these experiments, they are unlikely to tell us much about how it works.

We also found, as before (Berg and Turner, 1993; Berry et al., 1995), that motors driven backward at speeds up to a few tens of Hertz, often broke catastrophically. Cells pushed forward with similar applied torque rotated at speeds up to approximately 50 Hz, and did not break catastrophically. If there are no barriers to backward rotation, and if motor torque is independent of speed up to a few hundred Hertz at room temperature (Berg and Turner, 1993), then the average torque experienced by the motor is similar in either case. So why should motors break when rotating slowly backward but not when rotating forward? Perhaps the torque in a motor driven backward is transiently much higher than in a motor running forward, even though the average torque is similar. This possibility should be addressed in future models of the motor mechanism.

We are in the process of reconstructing an optical trap (Block et al., 1989) that can be used to conduct an electrorotation-independent test for the existence of barriers to backward rotation. With a carefully designed experiment, we hope to remove any angular dependence in the applied torque. If the variation in motor torque is small and there is no barrier, we would expect to be able to drive a cell backward with a trap strength virtually identical to that required to stop it from rotating forward. Alternatively, we should be able to detect and measure any significant angular variation in motor torque that might exist. In any event, the

analysis presented here demonstrates that great care is necessary in interpreting experiments in which the motions of molecular motors are observed and manipulated via flexible linkages to much larger objects such as cells, glass needles, or beads. This is equally true for experiments with eukaryotic motors, such as myosin, kinesin, or RNA polymerase, as has been shown recently for myosin (Molloy et al., 1995).

We thank Aravi Samuel, Alan Stern, and Linda Turner for their comments on the manuscript.

R. M. Berry is the recipient of a Wellcome Trust International Prize Traveling Research Fellowship. This work was supported by the Rowland Institute for Science.

REFERENCES

Berg, H. C., and L. Turner. 1993. Torque generated by the flagellar motor of *Escherichia coli*. *Biophys. J.* 65:2201–2216.

Berry, R. M., L. Turner, and H. C. Berg. 1995. Mechanical limits of bacterial flagellar motors probed by electrorotation. *Biophys. J.* 69: 280–286.

Blair, D. F., and H. C. Berg. 1988. Restoration of torque in defective flagellar motors. *Science.* 242:1678–1681.

Block, S. M., and H. C. Berg. 1984. Successive incorporation of force-generating units in the bacterial rotary motor. *Nature.* 309:470–472.

Block, S. M., D. F. Blair, and H. C. Berg. 1989. Compliance of bacterial flagella measured with optical tweezers. *Nature.* 338:514–517.

Coulton, J. W., and R. G. E. Murray. 1978. Cell envelope associations of *Aquaspirillum serpens* flagella. *J. Bacteriol.* 136:1037–1049.

Khan, S., T. S. Reese, and M. Dapice. 1988. Effects of Mot gene expression on the structure of the flagellar motor. *J. Mol. Biol.* 202:575–584.

Lowe, G., M. Meister, and H. C. Berg. 1987. Rapid rotation of flagellar bundles in swimming bacteria. *Nature.* 325:637–640.

Macnab, R. M. 1996. Flagella and motility. *In Escherichia coli* and *Salmonella:* Cellular and Molecular Biology, 2nd ed. F. C. Neidhardt, R. Curtiss III, J. L. Ingraham, E. C. C. Lin, K. B. Low, B. Magasanik, W. S. Reznikoff, M. Riley, M. Schaechter, and H. E. Umbarger, editors. American Society for Microbiology, Washington, D. C. 123–145.

Meister, M., S. R. Caplan, and H. C. Berg. 1989. Dynamics of a tightly coupled mechanism for flagellar rotation. *Biophys. J.* 55:905–914.

Molloy, J. E., J. E. Burns, J. Kendrick-Jones, R. T. Tregear, and D. C. S. White. 1995. Movement and force produced by a single myosin head. *Nature.* 378:209–212.

Silverman, M., and M. Simon. 1974. Flagellar rotation and the mechanism of bacterial motility. *Nature.* 249:73–74.

Washizu, M., Y. Kurahashi, H. Iochi, O. Kurosawa, S.-I. Aizawa, S. Kudo, Y. Magariyama, and H. Hotani. 1993. Dielectrophoretic measurement of bacterial motor characteristics. *IEEE Trans. Ind. Appl.* 29:286–294.